Materials Advances

ROYAL SOCIETY OF CHEMISTRY

PAPER

View Article Online
View Journal | View Issue

Cite this: *Mater. Adv.*, 2025, 6, 3903

Optimized PEGylated cubosomes: a novel approach for specific delivery of dacomitinib to non-small cell lung cancer cells

Mohamed Nasr, *[ab] Rania Mokhtar[a] and Rania S. Abdel-rashid [a]

Dacomitinib (DM), a newly FDA-approved chemotherapeutic agent, demonstrates remarkable selectivity in combating non-small cell lung cancer (NSCLC) and hindering its severe metastasis. This study aimed to engineer pH-triggered drug-release of PEGylated cubosomes for the delivery of DM to improve its targeting potential with minimal side effects. Eight PEGylated cubosomal dispersions were prepared using the emulsification method using a 2^3 full factorial design. The prepared dispersions were characterized for their particle size, entrapment efficiency, zeta potential, and drug release at pH 7.4 and 5.5. The optimized formula was subjected to further investigations such as XRD, DSC, TEM, FTIR, *in vitro* cytotoxicity, cellular uptake, and flow cytometry. The optimum DM-loaded PEGylated cubosomes displayed a mean particle size of 214.30 ± 0.41 nm, PDI of 0.231 ± 0.001, and drug entrapment efficiency of 95.04% ± 0.40%. The cumulative % release of DM after 24 h at pH 7.4 and 5.5 was 6.30% ± 0.33% and 70.00% ± 1.01%, respectively, confirming pH-triggered release. *In vitro* cytotoxicity study highlighted the potent cytotoxic effect of DM-loaded PEGylated cubosomes against the H-1975 cell line, as indicated by a significantly ($P < 0.05$) reduced IC_{50} value by approximately 7.70-fold compared with that of pure DM. The overall cellular uptake of DM-loaded PEGylated cubosomes was immensely significant compared with a negligible uptake of the free drug, in addition to causing apoptotic cell death in the G1/S phase. Results demonstrated that DM-loaded PEGylated cubosomes could be ranked as an efficiently selective delivery system for transporting DM to a human lung cancer mutant cell line.

Received 12th December 2024,
Accepted 26th April 2025

DOI: 10.1039/d4ma01232a

rsc.li/materials-advances

1. Introduction

Cancer continues to be a leading health challenge worldwide. Lung cancer ranks as the second deadliest cancer globally. Recently published statistics from the American Cancer Society stated that there were 238 340 new lung cancer cases in the United States in 2023.[1] Nearly 85% of them were diagnosed with non-small cell lung cancer (NSCLC), which is regarded as the ubiquitous lung cancer type, with metastatic manifestations in almost 65% of these cases when firstly diagnosed.[2,3]

Tyrosine kinase causes protein phosphorylation in normal cells, leading to activation of sensors that regulate cell proliferation, apoptosis, and angiogenesis. Mutations may evolve within tyrosine kinases, disrupting signal transmission and thereby leading to tumor development. Receptors such as epidermal growth factor receptors (EGFRs) have a significant impact on cancer propagation and vasculogenesis.[4] Therefore, inhibiting these receptors can halt signaling pathways, ultimately preventing cancer prognosis. The utilization of small molecule tyrosine kinase inhibitors (TKIs) can compete with ATP for binding to proteins' tyrosine kinase domains to block protein phosphorylation and inhibit proliferation and carcinogenic signals.[5,6] This approach is highly significant and is regarded as the primary first-line therapy for lung cancer cases, particularly those showing progressive NSCLC with specific *EGFR* gene mutations.[7]

Numerous clinical trials have shown that TKIs are effective in enhancing progression-free survival (PFS) compared with other treatment methods.[8] First-line TKIs targeting the EGFR, such as erlotinib and gefitinib, initially showed robust efficacy against these mutations. However, resistance often develops as a result of mutation in the EGFR kinase domain (T790M). This mutation is responsible for about 50–60% of acquired resistance, abolishing the effectiveness of first-generation TKIs by altering the pocket for ATP-binding, and preventing the binding of EGFR and TKI. To address this mutation-based resistance, subsequent generation of irreversible EGFR TKIs have evolved, like afatinib and DM.[4,9]

[a] *Pharmaceutics and Industrial Pharmacy Department, Faculty of Pharmacy, Helwan University, Ain Helwan, Cairo 11795, Egypt. E-mail: m2nasr@yahoo.com, Rania.AliMohamed@Pharm.helwan.edu.eg, sansoova@yahoo.com, Rania.safa@pharm.helwan.edu.eg; Tel: +2 01001668824*
[b] *Department of Pharmaceutics, Faculty of Pharmacy, Delta University for Science and Technology, Gamasa 11152, Egypt*

FDA approved DM (marketed as VIZIMPRO® tablets in 2018) is a first-line therapy for patients with metastatic NSCLC that have EGFR mutations (exon 19 deletion or exon 21 L858R substitution mutations).[10,11] DM has exhibited high efficiency as a remedy for resistant lung cancer. However, its clinical application is hindered by some adverse reactions such as severe diarrhea, rash, stomatitis, and decreased appetite due to oral delivery. Also, DM is known to present a high protein binding of 98% and it is pH sensitive; therefore, encapsulation in nanoparticles or lipid-based carriers may potentially reduce its protein binding and enhance its distribution to target tissues. Therefore, there is an unmet need for a novel approach to deliver DM to the cancer zone effectively and minimize adverse effects.[12]

Nanoscale drug delivery has been extensively studied in the battle of cancer treatment with their advantages including the feasibility to target tumors, low toxicity to healthy cells, and reduced effective doses. Nanotherapeutics can also guard drugs against degradation by extracellular enzymes and bypass clearance mechanisms to improve cellular uptake and targeted delivery to specific sites.[13–15] Various types of nanoparticles were fabricated to respond to stimuli such as pH changes, reducing agents, light, and enzyme activities and have gained significant consideration in the cancer therapy field. The pH-sensitive nanoformulations can be engineered to selectively release drugs in specific physiological compartments, such as tumor microenvironments, where pH levels may differ from normal tissues (6.5 to 6.9 extracellularly and 5.0 to 5.5 intracellularly). Thus, pH-responsive nanoparticles may offer a promising approach for treating cancer.[16] Incorporating biocompatible polyethylene glycol (PEG) chains onto the nanoparticle surface is a widely adopted method to enhance drug efficacy by extending its circulation in the body. PEG prevents opsonins from binding to the nanoparticles through steric hindrance, thereby shielding them from phagocytic elimination.[17] Polyethylene glycol 6000 (PEG 6000) is a hydrophilic polymer that is often incorporated into drug delivery systems to enhance solubility, stability, and mucoadhesion. In cubosome formulations, PEG 6000 can stabilize the nanoparticles, prevent aggregation, and potentially prolong systemic circulation through steric stabilization effects.[18,19]

Cubosomes are lipid-based nanoparticles that have harvested significant attention for drug transport due to their exceptional structure and potential for targeted therapy.[20,21] Glyceryl monooleate (GMO) is a biocompatible, amphiphilic lipid widely used in cubosome formulations due to its ability to self-assemble into bicontinuous cubic phases in the presence of water. This unique structural arrangement provides a high surface area and enhances drug solubilization, making it suitable for lipophilic and poorly water-soluble drugs.[22] Incorporating oleic acid (OA) into cubosomes offers a promising strategy to enhance their selectivity for tumor cells.[23,24] Oleic acid (OA) is a long-chain unsaturated fatty acid that serves multiple functions in lipid-based delivery systems. It enhances membrane fluidity and drug encapsulation,[23] and improves cellular uptake. Cancer cells generally have an upregulated lipid metabolism, partly due to their rapid proliferation rates. Oleic acid exploits this metabolic difference by targeting the cancer cells' lipid uptake pathways, enhancing the selectivity of the cubosomes for cancer cells and improving targeted delivery of DM. Incorporating oleic acid into cubosomes can enhance their responsiveness to the acidic tumor microenvironment, resulting in more efficient drug release in the slightly acidic pH of tumor tissues compared with the neutral pH of normal tissues.[23,25] Previous studies indicate that oleic acid may possess antitumor properties, potentially affecting key pathways involved in cancer cell proliferation and survival.[26,27] This study aimed to develop a pH-sensitive PEGylated cubosomal formulation incorporating oleic acid to enhance the targeted delivery of dacomitinib (DM) to the acidic tumor microenvironment of NSCLC while minimizing systemic exposure and off-target effects. To achieve this goal, the amounts of glyceryl monooleate (GMO), oleic acid (OA), and PEG 6000 will be optimized using Design-Expert® statistical estimation. The optimized formula will be subjected to further investigations such as XRD, DSC, TEM, FTIR, *in vitro* cytotoxicity, cellular uptake, and flow cytometry.

2. Materials and methods

2.1. Materials

Glyceryl monooleate (GMO) was kindly given as a gift by Gattefosse (Lyon, France). DM, poloxamer 407 (P 407), and HPLC grade ethanol, acetonitrile, and orthophosphoric acid were sourced from Sigma Aldrich (Steinheim, Germany). Oleic acid (OA) and PEG 6000 were obtained from Al-Gomhoria Company for Medicines and Medical Supplies (Cairo, Egypt). De-ionized water was acquired from Chemajet (Cairo, Egypt). All other chemicals used were of HPLC analytical grade.

2.2. Experimental design

A complete 2^3 factorial design was created by Design-Expert® software (version 13.0.5.0, Stat-Ease, Inc., Minneapolis, MN, USA). In Table 1, the experimental setup was detailed showing the independent factors (formulation parameters), and the examined dependent factors (four chosen responses). ANOVA

Table 1 Independent factors and responses of the 2^3 factorial design

	Levels	
Independent factors	Low	High
GMO (% w/w)[a]	2.5	5
GMO : OA molar ratio	2 : 1	4 : 1
PEG 6000 (% w/w)[b]	5	10
Responses	**Unit**	**Goal**
Particle size	Nm	Minimize
Entrapment efficiency	%	Maximize
Release at pH 7.4%	%	Minimize
Release at pH 5.5%	%	Maximize

[a] % w/w regarding the total weight of dispersion. [b] % w/w with respect to the total lipid weight.

Table 2 Composition of DM-loaded PEGylated cubosomes

Formula code	Amount (mg)					Total weight of dispersion (g)
	GMO	OA	PEG 6000	P 407	DM	
F1	500	250	37.50	75.00	20	20
F2	500	125	31.25	62.50	20	20
F3	500	250	75.00	75.00	20	20
F4	500	125	62.50	62.50	20	20
F5	1000	500	75.00	150.00	20	20
F6	1000	250	62.50	125.00	20	20
F7	1000	500	150.00	150.00	20	20
F8	1000	250	125.00	125.00	20	20

statistical analysis was employed to evaluate the factors significance in the best-fitting factorial model, with statistical significance set at $P < 0.05$. Surface response plots were utilized to visualize the interactions of the factors on the responses. Desirability was computed to aid in selecting the optimized formula for further evaluation.

2.3. Preparation of DM-loaded PEGylated cubosomes

As illustrated in Table 2, eight formulations of PEGylated cubosomes were generated using different ratios of GMO and OA following the procedures described by Nasr *et al.*[28,29] Briefly, GMO, OA, and PEG 6000 were melted at 60 °C using a magnetic stirrer (MSH-20D, Korea), then DM and P 407 were dispersed until a homogeneous mixture was formed. Hot deionized water (0.5 mL) was added in a dropwise manner while stirring at 500 rpm until homogeneity was achieved. The mixture was left to equilibrate at room temperature for 48 hours. The weight of the obtained gel was adjusted to a final weight of 20 g using deionized water and mixed thoroughly with a vortex mixer for 4 minutes, followed by sonication of the cubosomal dispersions for another 4 minutes using a probe sonicator (Dr Hielscher, Germany UP100H).

2.4. HPLC assay for quantification of DM

As DM was very recently approved by the FDA, few methods were reported for its analytical quantification. An accurate HPLC method for the determination of the drug in both formulation and dissolution media was reported by Kumari *et al.*[30] DM analysis *via* HPLC was performed using an Alliance system (e2695) from Waters, USA, equipped with a Waters UV/visible detector. A C18 stationary column (5 μm, 4.6 × 250 mm, Waters Corporation, Milford, MA, USA) was utilized and maintained at 35 °C where a mixture of acetonitrile and a buffer (75 : 25 ratio) was used as the mobile phase. The buffer was prepared by dissolving five mL of triethylamine in one liter of deionized water, adjusted to pH 3.20 ± 0.10 by orthophosphoric acid followed by micropore filtration through a 0.22 μm membrane filter and degassing by sonication. Data acquisition was managed using Empower 2 software. Chromatographic examination at 254 nm was performed in isocratic elution mode at a flow rate of 1 mL min^{-1}. Samples were injected manually with an injection volume of 30 μL. The method was evaluated for linearity, accuracy, and precision, both within a single day (intra-day) and across multiple days (inter-day).

2.5. *In vitro* characterization of cubosomal formulations

2.5.1. Particle characteristics. The particle size, polydispersity index (PDI), and zeta potential of all cubosomal nanoparticles were measured using a Malvern Zetasizer (Malvern Instruments/Worcestershire, UK). A one mL sample from each nanoformulation was diluted with 29 mL of deionized water and measurements were performed in triplicate at 25 ± 0.5 °C.

2.5.2. Entrapment efficiency (% EE). The mean percentage of DM successfully loaded in each formulation was determined as the average of three trials.[28,31] Entrapment efficiency (% EE) was assessed by quantifying the total and free (non-entrapped) DM. To measure the total DM content, 9 mL of ethanol was added to 1 mL of the prepared cubosomal dispersion, and the resulting solution was analyzed. To determine the free non-entrapped DM, an ultrafiltration centrifugation technique was used, where 3 mL of DM-loaded PEGylated cubosomes were diluted to 10 mL with deionized water and centrifuged at 5000 rpm using Ultra 3000 Amicon MWCO centrifuge tubes (Millipore, USA). Both total and free DM concentrations were quantified using HPLC at 254 nm, as previously described. Entrapment efficiency (% EE) was calculated using the following equation (per 1 mL sample):

$$\%\ \mathrm{EE} = \frac{\text{Total practical amount of drug} - \text{Amount of free drug in filtrate}}{\text{Total practical amount of drug}} \times 100$$

2.5.3. *In vitro* drug release study. The dialysis method was applied to investigate *in vitro* drug release from the prepared cubosomes.[32,33] Cellulose membrane dialysis tubing (20.4 mm × 32 mm, molecular weight cutoff 12 000–14 000 Da, Sigma-Aldrich, St. Louis, MO) was pre-soaked in deionized water overnight prior to the experiment. The drug release study was conducted over 24 hours in two different media. The first medium was phosphate buffer pH 7.4 to mimic blood conditions, and the second medium was adjusted to pH 5.5 to represent the tumor environment, as previously described.[34] Tween 80 (0.1%) was added to both buffers to conserve sink conditions. The cellulose tubing was filled with either 1 mg of DM dispersion at phosphate buffer or a volume of cubosomal dispersion equivalent to 1 mg of DM. The securely sealed cellulose tubes were immersed in the release media and stirred at 100 rpm and 37 °C. At stated time intervals (1, 2, 4, 6, 8, 12, and 24 hours), a known volume of the sample was withdrawn and instantly restored with a fresh medium. Samples were filtered through a syringe filter (0.45 μm) before HPLC analysis. The release behavior was studied in triplicate, and the resulting data was expressed as % cumulative drug released against time. The *in vitro* release profiles were analyzed using different models of kinetics, including zero order, first order, and Higuchi's model. The correlation coefficient (R^2) was calculated

for all models, and that with the highest R^2 value was chosen as the best-fitting model.

2.5.4. Optimized formulation prediction. The optimum DM-loaded PEGylated cubosomal preparation was anticipated based on data statistical analysis and various response optimizations deducted from the Design-Expert® program. The predicted formulation was elaborated and characterized for its particle size, efficiency of entrapment, and release after 24 h at pH 7.4 and pH 5.5. Moreover, the optimum DM-loaded PEGylated cubosomal formulation was subjected to the following characterizations.

2.5.5. X-Ray diffraction (XRD) studies. XRD analysis of the optimized cubosomes, blank cubosomes, and pure DM were performed using a Philips® X'pert multipurpose diffractometer (PANalytical, Netherlands). Cu was used as the tube anode, and diffractograms were recorded under 40 kV voltage, 30 mA current, and 0.02° step size with counting rate of 1 s per step at room temperature. The resulting values were collected over a scattering angle (2θ) range of 10–50°.

2.5.6. Differential scanning calorimetry (DSC). DSC analysis was conducted using a thermal analysis system (DSC-60, Shimadzu, Japan) to investigate potential physical changes in the DM within cubosome dispersions. Pure DM powder, blank cubosomes, and prepared cubosomal dispersions were analyzed. In an aluminum pan, approximately 5 mg of samples were exposed to a constant rate of heat (10 °C min^{-1} from 25 °C to 250 °C) under a nitrogen gas flow to prevent sample oxidation. An empty pan served as the reference during the analysis under a nitrogen atmosphere.[35]

2.5.7. Fourier-transform infrared (FTIR) spectroscopy. The physicochemical interaction of DM with cubosomal components was examined by recording the FTIR spectra of pure DM, blank cubosomes, and the optimized cubosomal formulation using an FTIR Shimadzu 8400S spectrophotometer, Lab Wrench, Japan. Each sample, weighing approximately 2–3 mg, was pressed into a disc by blending with dry potassium bromide followed by scanning across the range of 400–4000 cm^{-1}.[36]

2.5.8. Transmission electron microscopy (TEM). The morphology of the optimized DM-PEGylated cubosomal dispersion was analyzed using transmission electron microscopy (TEM) equipped with super twin lenses. A drop of a recently formulated sample diluted with deionized water was mounted on a copper mesh coated with copper, and allowed to dry out and adhere to the carbon coat. Subsequently, the sample was pigmented with 1% w/v phosphotungstic acid dye, then air-dried for 15 minutes at 25 °C. Then, the pigmented sample was examined and photographed using TEM (JEOL JEM-1400, Japan) at suitable amplifications.

2.6. *In vitro* pharmacological evaluations

2.6.1. Hemolysis test. Since the cubosomes were designed for intravenous administration, their impact on erythrocytes was studied.[37,38] The red blood cells were isolated from blood by centrifugation at 2000 rpm for 10 minutes at 4 °C and then dispersed in PBS to achieve a 2% (v/v) concentration. Next, 500 μL of the erythrocyte suspension was mixed with 500 μL of cubosomal dispersion equivalent to different concentrations of DM (50, 100, 150, 200, and 500 μg mL^{-1}). After 2 h at body temperature, the supernatant was centrifuged at 5000 rpm for 5 minutes, and the supernatant was spectrophotometrically examined at a wavelength of 570 nm. Deionized water and buffer solution served as the positive and negative control, respectively. In conclusion, the relative hemolysis rate (RHR%) was calculated using the provided equation:

$$\mathrm{RHR\%} = [(A_1 - A_0)/(A_2 - A_0)] \times 100$$

where A_0: the absorbance of the group treated with buffer; A_1: the absorbance of the group treated with an optimum cubosomal formulation; A_2: the absorbance of the group treated with deionized water.

2.6.2. *In vitro* cell culture studies. RPE-1 epithelial cells (normal cell line), A549 adenocarcinoma lung cells (no EGFR-TK mutations) and the human lung cancer EGFR mutant NSCLC cell line (H-1975) were obtained from the American Type Culture Collection. H-1975 was selected for the current *in vitro* study as it harbors both types of gene mutations, one that is sensitive to the drug (L858R), while the other coded T790M represented the resistant mutations of EGFR.[39] Cells were cultured using DMEM (Invitrogen/Life Technologies) supplemented with 10% FBS (Hyclone), 10 μg mL^{-1} of insulin (Sigma), and 1% penicillin–streptomycin, all stored at 37 °C/5% CO_2. The DM solutions were dissolved using DMSO. For accuracy, all experiments were performed three times.

2.6.2.1. In vitro assessment of cytotoxic potential. The *in vitro* cytotoxic potential of pure DM, DM-loaded PEGylated cubosomes, and blank PEGylated cubosomes was measured in RPE-1, A-549, and H-1975 cell lines using the MTT assay.[40] In 96-well plates, the different cell lines were seeded at a density of 1.2–1.8 $\times 10^4$ cells per well in 100 μL of complete growth medium and incubated at 37 °C for 24 h to allow attachment. The cells were incubated for 48 h with 100 μL of different concentrations (0.39, 1.56, 6.25, 25, and 100 μg mL^{-1}) of either DM solution, DM-loaded PEGylated cubosomes, or blank PEGylated cubosomes. MTT solution was added to each well at 10% of the culture medium volume. Following a further 4 hours of incubation, MTT solubilization solution was put in a volume equivalent to the original culture medium volume to dissolve the resulting formazan crystals. Background absorbance was detected at 690 nm, then subtracted from the values recorded at 450 nm using a microplate reader (Robonik P2000 Eia reader). The IC_{50} values were determined for each cell line by interpolation from the fitted sigmoidal curve. The selective index (SI) is a parameter commonly used in cytotoxic tests to assess the relative toxicity of a compound to target cells compared with non-target cells. Higher SI values indicate greater potential for selectivity.[41]

$$\mathrm{SI} = \mathrm{IC_{50}\ of\ the\ normal\ cells}/\mathrm{IC_{50}\ of\ tumor\ cells}$$

2.6.2.2. Cellular uptake of drug in H-1975 mutant lung cancer cell line. The internalization of the optimized formulation was

studied *in vitro* using H-1975 mutant lung cancer cell (L858R/T790M) monolayer cultures. At an estimated density of 5000 cells per well and 100 μL volume of medium, the H-1975 mutant lung cancer cells were sown in 96-well plates and allowed to adhere for 24 h before the experiment. The study was implemented on three distinctive cell line groups: the first one was treated with a concentration equivalent to IC_{50} of free DM, whereas the second one was treated with a similar concentration of the optimized DM-loaded PEGylated cubosomes.[42] Cells without any DM served as a blank control (group 3). After incubation for 12 hours, the growth media were collected, and the cells were washed thrice with PBS. DM concentrations in the collected media and PBS washes were analyzed using HPLC. The % cumulative intracellular DM was calculated based on the following equation:

$$\%\ \text{cumulative intracellular DM} = [(C_0 - C_{\text{exa}\,t})/C_0] \times 100,$$

where C_0 is the initial concentration of DM added to cells and $C_{\text{exa}\,t}$ is the extracellular concentration of DM at time = t.

2.6.2.3. Cell cycle analysis by flow cytometry. This assay is designed for the quantitative analysis of DNA content in tissue culture cells using propidium iodide (PI) for nucleic acid staining followed by flow cytometry analysis. H1975 cells (3×10^5 cells per well) were added in six-well plates. After one day of incubation at 37 °C in a 5% CO_2 atmosphere, the culture medium was substituted with freshly prepared medium including either free DM or the optimized DM-loaded PEGylated cubosomes at IC_{50} concentrations, followed by the incubation of cultured cells for another 24 hours. At the end of the incubation period, treated cell pellets were harvested and washed twice with PBS after centrifugation and the supernatant was discarded. The cell pellets were then resuspended in a mixture of PBS and fixed in 70% ethanol for 2 hours at 4 °C. A second centrifugation cycle was performed at 1000 rpm for 5 minutes, the supernatant was removed, and the cells were rehydrated with PBS. The produced cellular pellets were then kept within a mixture of propidium iodide and ribonuclease for 30 minutes before investigation. Data were presented as % relative to the untreated cell population.[37]

2.6.2.4. Cell apoptosis study by flow cytometry. The quantification of apoptotic cells was performed using a kit containing annexin V fluorescein isothiocyanate (V-FITC) and propidium iodide. Initially, H-1975 cells were seeded at a density of 4×10^5 cells per well in six-well plates overnight. They were then treated with fresh medium containing either free DM or the optimized DM-loaded PEGylated cubosomes for 24 hours. Subsequently, the cells were harvested by centrifugation (1000 rpm, 5 minutes), resuspended in a buffer solution, and stained with V-FITC and PI following the kit's protocol. The stained cells were incubated at room temperature for 5 minutes in the dark, and apoptotic cells were quantified using flow cytometry. Living cells, early apoptotic cells, late apoptotic cells, and necrotic cells were identified as Q1, Q2, Q3, and Q4, respectively.

3. Results and discussion

3.1. HPLC assay of DM

The HPLC assay demonstrated excellent linearity for DM concentrations ranging from 0.5 to 20 μg mL^{-1}, with a regression coefficient (R^2) of 0.999. The mean percentage recovery varied between 99.87% and 99.6%, demonstrating the assay's high accuracy. The interday and intraday precision ranged from 100.28% and 98.5%. Additionally, the relative standard deviation (RSD) for all was below 2%, indicating a high level for the assay.

3.2. Factorial design data analysis

A 2^3 complete factorial designed study was implemented to examine the impacts of three independent factors: GMO% (X1), OA % (X2), and PEG 6000 (X3) at two levels on particle size (Y1), EE % (Y2), % release after 24 h at pH 7.4 (Y3) and 5.5 (Y4). The results for every response were analyzed using Design Expert® software, with ANOVA used to assess the influence of the independent variables on the responses, considering $P < 0.05$ for statistical significance. The software identified the best fitting model (linear, 2F1, and/or quadratic) for every response depending on the predicted and adjusted R^2 values.

3.2.1. Effect on particle size. The mathematical mean particle size of the formulated cubosomal dispersions ranged between 201.30 ± 1.22 and 221.20 ± 0.7 nm as detailed in Table 3. The linear regression model was identified as significant for representing the particle size response (Y1). ANOVA statistical analysis revealed that GMO% (X1) had a statistically significant effect on particle size ($P < 0.05$), whereas OA (X2) and PEG 6000 (X3) did not show significant effects (Fig. 1(A)).

Table 3 Particle size, PDI, zeta potential, % EE, % DM release of DM-loaded PEGylated cubosomal formulations after 24 h at pH 7.4 and 5.5

	Mean ± SD					
					% cumulative release after 24 h.	
	Particle size (nm)	PDI	Zeta potential (mV)	EE (%)	pH 7.4	pH 5.5
F1	203.40 ± 1.63	0.255 ± 0.01	−34.80 ± 1.06	85.6 ± 0.90	8.79 ± 0.41	98.60 ± 1.63
F2	205.40 ± 1.31	0.174 ± 0.02	−33.20 ± 0.24	80.3 ± 1.06	8.85 ± 0.49	85.00 ± 1.63
F3	209.90 ± 1.22	0.247 ± 0.02	−33.70 ± 0.33	81.38 ± 0.73	8.67 ± 0.57	90.24 ± 2.45
F4	201.30 ± 1.22	0.266 ± 0.02	−32.40 ± 0.65	82.10 ± 1.64	9.4 ± 0.82	80.00 ± 2.00
F5	214.30 ± 0.41	0.231 ± 0.001	−33.00 ± 0.16	95.04 ± 0.41	6.3 ± 0.33	70.00 ± 1.01
F6	221.20 ± 0.73	0.238 ± 0.10	−33.70 ± 0.41	90.08 ± 0.24	7.1 ± 0.73	55.10 ± 1.31
F7	218.30 ± 0.90	0.249 ± 0.05	−31.20 ± 0.73	93.07 ± 0.49	6.8 ± 0.65	60.00 ± 0.82
F8	220.00 ± 1.14	0.312 ± 0.17	−34.90 ± 0.49	92.60 ± 0.33	7.1 ± 0.98	53.20 ± 1.14

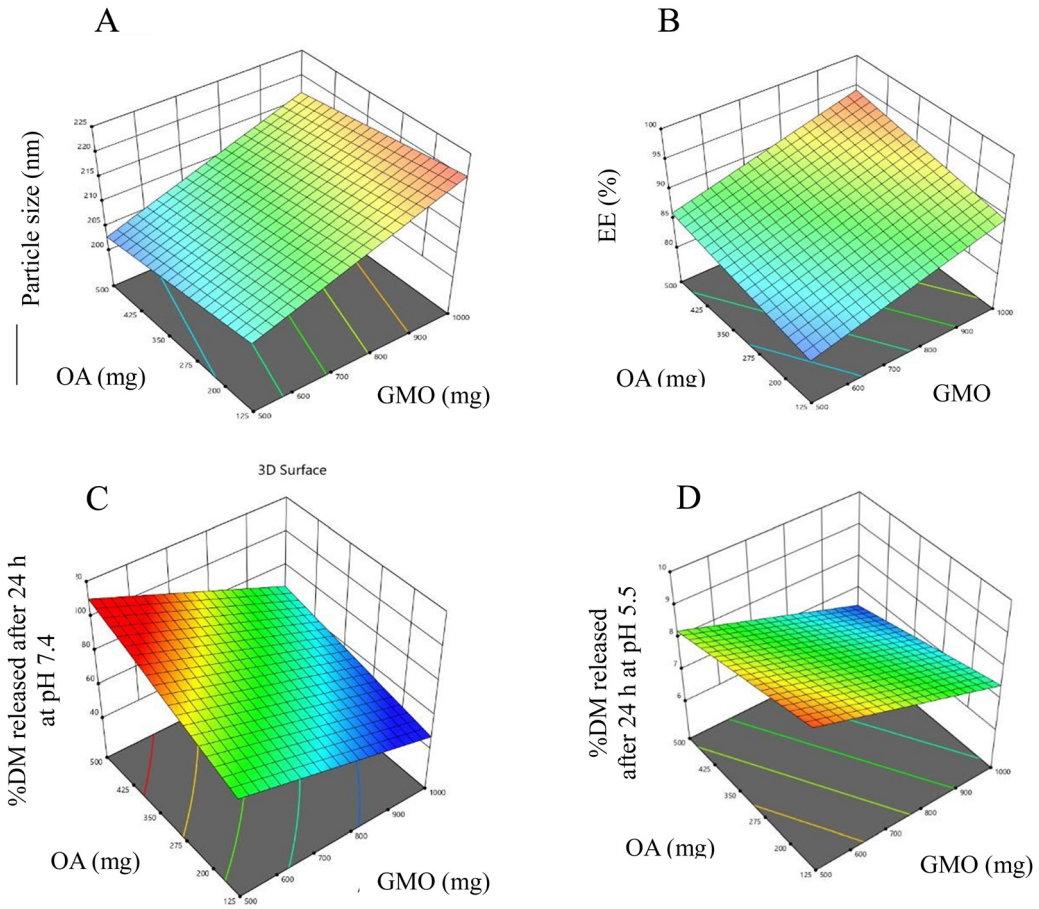

Fig. 1 The 3-D response surface plots for the influence of the independent factors on (A) the particle size, (B) % EE, and (C) % release after 24 h at pH 7.4 and (D) at pH 5.5.

An increase in the concentration of GMO from 2.5% to 5% caused an increase in the particle size. The increased lipid content results in larger cubosomes as more material is available to form the bilayers and internal structure.[28] PEG chains provide steric stabilization by forming a hydrophilic layer around the cubosomes, which prevents aggregation and may cause an increase in particle size.[43] OA can physically insert itself between the lipid molecules in the bilayer, leading to a more loosely packed structure. This can enhance the flexibility and curvature of the bilayers, facilitating the formation of smaller particles.[44] The numerical values of PDI ranged from 0.174 ± 0.02 to 0.312 ± 0.17, as shown in Table 3, which is considered satisfactory for lipid-based delivery systems, indicating nanoparticulate size uniformity in the generated dispersions with minimal cluster formation.[35] The polynomial equation to estimate the mean particle size is described below:

$$\text{Particle size} = 211.77 + 6.98X_1 - 1.99X_2 + 1.70X_3$$

The zeta potential was measured to determine the surface charge of cubosomal nanoparticles, which is crucial for predicting long-term stability. The zeta potential results indicated that DM cubosomes had a negative charge, with mean values ranging from −31.20 ± 0.73 to −34.90 ± 0.49, as shown in Table 3. The negative surface charge on DM-loaded PEGylated cubosomes may be due to the ionization of the carboxylic group of the OA included in the formulation or the natural negative charge in GMO, or the presence of a polarized water layer surrounding the outer surface of the cubosomes.[45] The presence of P 407 as a stabilizer provided strong steric stability by preventing aggregation through steric hindrance.

3.2.2. Effect on the entrapment efficiency. The % EE ranged from 80.3 ± 1.06 to 95.04 ± 0.41, as indicated in Table 3. Derived from ANOVA statistical analysis, the linear model was the most suitable for predicting % EE. The results revealed that X1 (GMO%) significantly impacted % EE, whereas X2 (OA) and X3 (PEG 6000) were statistically insignificant, as depicted in the 3D response surface graphs (Fig. 1(B)). It was proposed that DM was 'grabbed' into the cubosomal nanoparticle's structure due to the high affinity of DM to the hydrophobic matrix of cubosomal nanoparticles. The high drug entrapment efficiency is advantageous for providing a therapeutic effect with a lesser volume.[33,46] The polynomial equation representing the % EE is shown as follows:

$$\%\ \text{EE} = 87.82 + 4.16X_1 + 2.42X_2 - 0.4597X_3$$

3.2.3. Effect on DM release at pH 7.4 and 5.5. The statistical analysis showed that the linear model was the most fitted model for predicting % release of DM at pH 7.4 while the model known as two-factor interaction (2FI) was chosen for evaluating the release at pH 5.5. The results were further analyzed by the 3-D response graph (Fig. 1(C) and (D)) and ANOVA statistical analysis. It was estimated that all the model terms and their interactions had a significant impact on the drug release. It could be concluded that increasing the concentration of either GMO or OA significantly lowered DM release from cubosomal nanoparticles due to an increase in matrix viscosity which delayed diffusion of the drug from the lipidic bilayer to the release medium.[47] The polynomial equations to estimate the release at pH 7.4 and pH 5.5 are described below:

$$\text{Release at pH 7.4} = 7.85 - 0.9060X_1 - 0.5077X_2 + 0.2501X_3$$

$$\text{Release at pH 5.5} = 75.19 - 17.64X_1 + 13.99X_2 - 8.91X_3 - 3.61X_1X_2 + 5.53X_1X_3 - 4.57X_2X_3$$

All cubosomal formulations showed a biphasic pattern at both pH 7.4 and 5.5 as shown in Fig. 2(A) and (B). An initial burst release occurs within the first 2 h, followed by steady release throughout 24 h, which is consistent with previously reported data.[22,48] This biphasic release is clinically significant, as the first burst release results in a speedy onset of action, but the sustained steady drug release allows for reduced dose frequency. The early burst impact may be due to the drug allocated onto the cubosomal nanoparticle's surface, whereas the following sustained release pattern may be related to the drug integrated into the cubosomal core and its dissemination through the pathways and channels formed within the cubic shaped nanoparticles.[49]

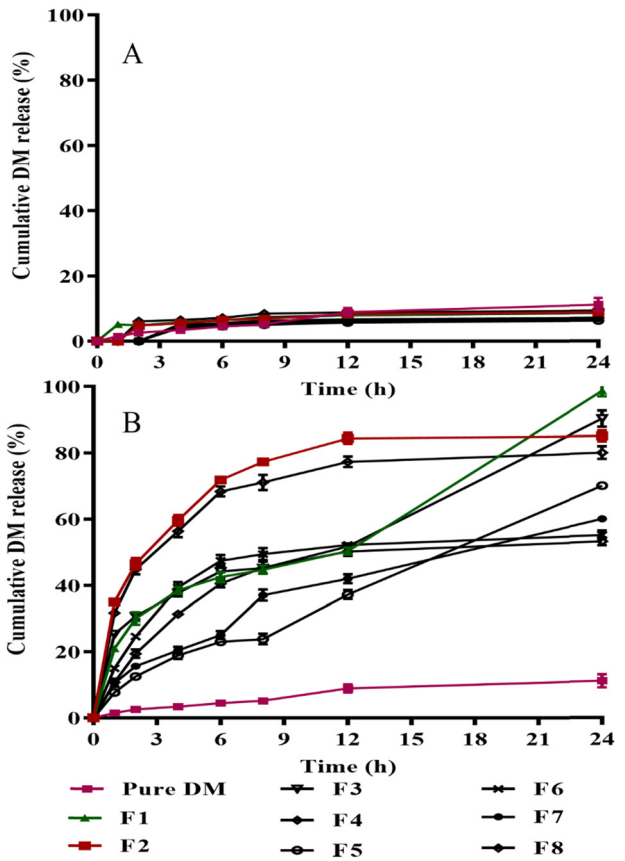

Fig. 2 *In vitro* release profiles of DM-loaded PEGylated cubosomal formulations (F1)–(F8) in PBS pH 7.4 (A) and pH 5.5 (B) at 37 ± 0.5 °C (n = 3; the values are stated as the mean ± SD).

The findings presented in Table 3 and Fig. 2(A) and (B) showed that the cumulative release was significantly decreased at normal physiological pH 7.4, reaching less than 9% of encapsulated DM in all formulations, which is ten times lower than the % of DM released at pH 5.5. This observation could have two different rationales. First, the higher dissolution of DM in acidic pH compared with normal biological pH may have played a role. Secondly, phase inversion and destabilization of cubosomes might have occurred, resulting in drug leakage from the nanoparticles. All formulas contain OA, which contains sufficient unsaturated fatty acid conjugated with the same acyl chain as GMO are considered beneficial for the fabrication of pH-responsive nanomedicines where the studies discovered that drug release of the diffusion-dependence nature is highly affected by the mesophase structure and the capacity of the water channels available inside the cubosomal nanoparticle.[50–52] The impact of OA on the phase behavior of hydrated GMO/OA mixtures is influenced by pH and salt concentration, as OA can alter its protonation state at different pH levels.[25,53] As a result, changes at pH can alter the structures of cubosomes, resulting in an increased release of DM in the acidic tumor microenvironment, while the drug release speed would be reduced at normal physiological pH.[54]

The *in vitro* release data were analyzed using various kinetic models and found to best fit the Higuchi model. This result suggests that DM release from cubosomes occurs *via* a diffusion mechanism, as indicated by the high regression coefficients (R^2). The adherence to the Higuchi model could be attributed to the structural characteristics of cubosomes, which possess a mesoporous structure with interconnected aqueous channels. In this configuration, the drug is typically dispersed within the lipid matrix, and its release and diffusion are driven by the concentration gradient through the cubic phase.[47,55]

3.3. Optimization of DM-loaded cubosomal dispersion

Numerical optimization using a desirability approach was conducted to optimize the formulation. Based upon the constraints listed in Table 4, the software Design-Expert® identified F5 as an optimal formulation, achieving the highest desirability value of 0.754, as illustrated in Table 4. Accordingly, F5 underwent further evaluation.

3.4. Transmission electron microscopy (TEM)

The photomicrograph of DM-loaded PEGylated cubosomal nanoparticles (F5) depicts cubic particles exhibiting the characteristic structure typical of cubosomes (Fig. 3). Moreover,

Table 4 The desirability grades of the developed formulations

Formula	Desirability
F1	0.301
F2	0.169
F3	0.253
F4	0.130
F5	0.754
F6	0.429
F7	0.594
F8	0.187

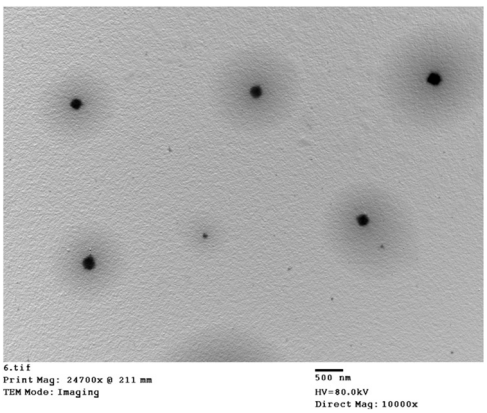

Fig. 3 TEM photomicrograph of DM-loaded PEGylated cubosomal nanoparticles (F5).

DM-loaded PEGylated cubosomal nanoparticles are observed to be well-separated from each other, indicating their stability.

3.5. X-ray diffraction (XRD)

XRD patterns of pure drug, plain cubosomes, and the optimized formula (F5) are illustrated in Fig. 4. The diffractogram of pure DM exhibited small peaks with low intensity, reflecting its low degree of crystallinity or amorphous state. This finding aligns well with the results reported by Druvasarika *et al.*[56] The diffractogram of blank cubosomes showed peaks that can be attributed to partially ordered components. This confirms that DM has been successfully encapsulated within the cubosomal matrix, likely existing in a molecularly dispersed or amorphous state within the lipid-based system.

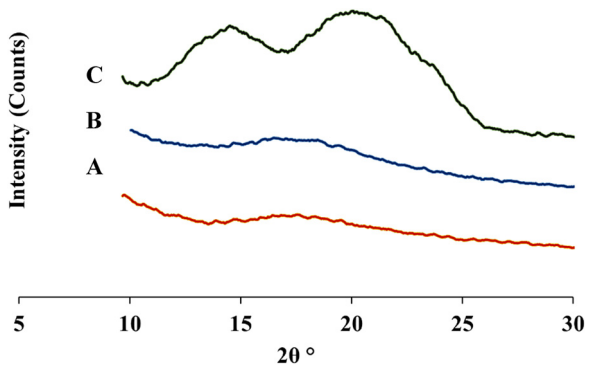

Fig. 4 XRD diffractograms of DM (A), plain (B), and DM-loaded PEGylated cubosomes (C).

3.6. Differential scanning calorimetry (DSC)

The differential scanning calorimetry (DSC) results align with the XRD findings. Fig. 5 displays DSC thermograms of DM, plain cubosomes, and DM PEGylated cubosomes (F5). The thermogram of pure DM displayed an endothermic peak at 182 °C, representing its melting temperature.[56] In contrast, this peak was absent in the DSC thermogram of F5, suggesting that DM may be dispersed in a molecular dimension within the cubosomal nanoparticles or due to in amorphous state[22] The thermogram of blank cubosomes exhibits broad endothermic transitions due to the lipid components, further supporting the structural integrity of the formulation.

3.7. Fourier transform infrared spectroscopy (FTIR)

The potential interactions between DM and the cubosomes were investigated using FTIR (Fig. 6). The FTIR spectrum of DM exhibits characteristic peaks, including N–H stretching (around 3300–3500 cm^{-1}) indicative of primary and secondary amine bonds and aromatic C=C stretching (1450–1600 cm^{-1}) typical of aromatic ring systems. Some characteristic peaks of DM were observed in regions overlapping with the cubosomal components, possibly due to the drug's encapsulation within the cubosomal layers.[57] The reduction in the intensity of certain characteristic peaks is attributed to the dilution effect during

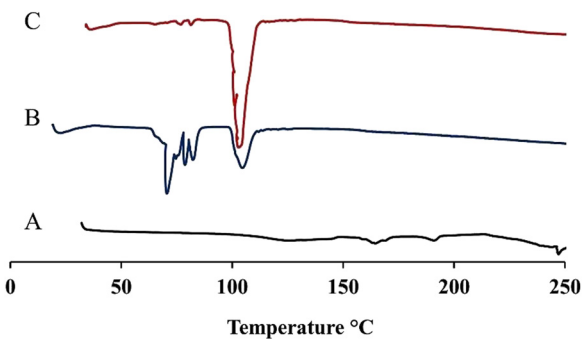

Fig. 5 DSC thermograms of DM (A), blank PEGylated cubosomes (B), and the optimized formula of DM-loaded PEGylated cubosomal nanoparticles (C).

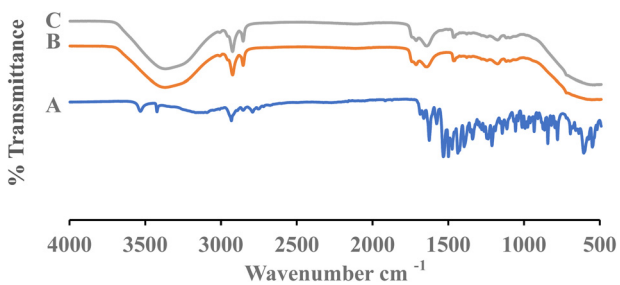

Fig. 6 FTIR spectra of DM (A), blank PEGylated cubosomes (B), and optimized formula of DM-loaded PEGylated cubosomal nanoparticles (C).

the formulation of DM-PEGylated cubosomes. This suggests the absence of significant chemical interactions.[22]

3.8. Hemolysis test

To assess the biosafety and biocompatibility of the formulated cubosomes, an *in vitro* hemolysis test was conducted using different concentrations of the optimized formulation (F5) compared with blank PEGylated cubosomes. Fig. 7 demonstrates negligible hemolysis across varying concentrations, with the relative hemolysis rate remaining below 2% even at a concentration of 500 μg mL^{-1}. These results indicate that the cubosomal dispersion formulation exerts minimal impact on erythrocytes and is suitable for injection. Previous studies have documented comparable outcomes.[48,58,59] The parenteral administration of DM is significantly more advantageous compared with the oral route.[60] This preference is primarily due to the skin and gastrointestinal toxicities associated with the newly developed generation of EGFR TKIs, which often necessitate dose modification and discontinuation when administered orally.[61] Also, the cubosomal surface was covered with PEGylation, which may eliminate any potential expected hemolytic effect and prevent the interaction with the membranes of RBCs.[62] Moreover, cubosomes stabilized by P 407 are less likely to disrupt the RBC's cell membrane.[63]

3.9. *In vitro* cell culture studies

3.9.1. *In vitro* cytotoxicity assay. To confirm the efficacy and selectivity of the optimized formulation (F5), three different cell lines were exposed to various concentrations (0.39, 1.56, 6.25, 25 and 100 μg mL^{-1}) of DM solution, DM-loaded PEGylated cubosomal dispersion, and equivalent concentrations of blank cubosomal dispersion, including normal epithelial cells (RPE1), human lung cancer cells (A-549), and mutant cell line (H-1975). The cell viability was then tracked using the MTT assay. All the results of IC_{50} values presented in Table 5 were statistically significant ($P < 0.05$) and indicated that blank cubosomes exhibited minimal toxicity for all tested cell lines, affirming the safety of these carriers. GMO lipid is extensively used in the food industry and is generally recognized as safe (GRAS), known for its relatively safe profile and reduced cytotoxicity.[31] On the other hand, DM-loaded PEGylated cubosomes and free DM demonstrated strong cytotoxic effects against both A-549 and H-1975 cancer cell lines.

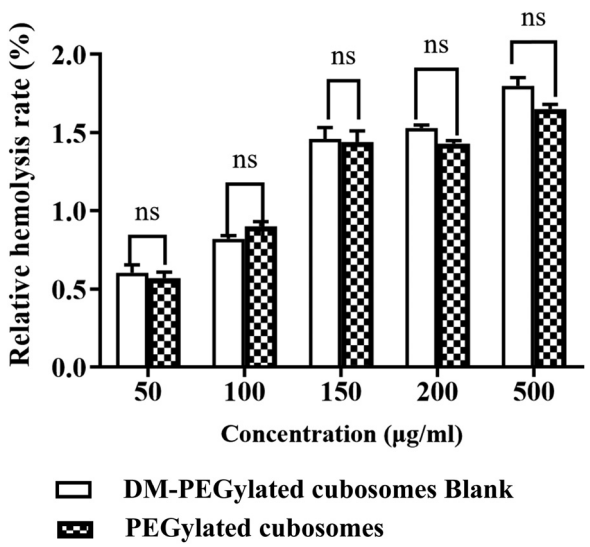

Fig. 7 Relative hemolytic rate of DM-loaded PEGylated cubosomes compared with blank PEGylated cubosomes.

However, the IC_{50} value of free DM in the A-549 cell line was found to be 2-fold higher than that exhibited by DM-loaded PEGylated cubosomes (20.40 and 10.2 μg mL^{-1}, respectively). Moreover, in the case of H-1975 cells, the IC_{50} values were 16.29 and 2.11 μg mL^{-1}, respectively with almost a 7.7-fold decrease in the mean IC_{50} value of DM-loaded PEGylated cubosomes compared with free DM. The previous results highlighted the active targeting ability mediated by the cubosomes based on their lipidic and cell-penetrating nature. It could also be observed that the IC_{50} of DM-loaded cubosomes in the H-1975 cell line is significantly lower compared with its IC_{50} in the case of human lung cancer cells (A-549). This could be attributed to the direct action of DM on non-small cell lung cancer mutated cells.[64] In contrast, the IC_{50} of free DM was 31.30 ± 1.50 μg mL^{-1} in RPE1 normal epithelial cells, while the mean IC_{50} was significantly increased to 163.30 ± 3.70 μg mL^{-1} ($P < 0.05$) after its incorporation into cubosomal nanoparticles. These results reflect the selectivity and targeting ability of DM-loaded cubosomes towards cancerous cells compared with normal cells. These findings correlated well with the results of *in vitro* DM release studies. Meanwhile, the cumulative drug release after 24 h was $6.30 \pm 0.33\%$ in normal physiological pH conditions, which is significantly lower than the $70.00 \pm 1.01\%$ in the acidic microenvironment (pH 5.5). Moreover, the calculated SI of DM-loaded PEGylated cubosomes to H-1975 cells compared with normal cells was found to be 77.39 (Table 5), indicating the highly potent cytotoxic effect of the optimized F5 against the metastatic NSCLC harboring EGFR mutations. Collectively, the results confirmed the efficient selectivity and targeting potential of the formulated DM-loaded PEGylated cubosomes.

The morphological changes in cell lines were visualized by an inverted microscope (magnification = 400×) after 48 h incubation with the different concentrations of DM-loaded cubosomes as shown in Fig. 8. The optical images of control samples showed that the cells in all three cell lines were intact with clear outlines. On the contrary, after the addition of the least concentration of DM-loaded cubosomes on H-1975 cell lines, the cells lost their normal sheet-like growth and most of the remaining few cells appeared degenerated. The same effect appeared at higher concentrations in the A-549 cell line while cell death and degeneration only started to appear at 100 μg mL^{-1} in RPE 1 normal cells.

3.9.2. Cellular uptake and drug accumulation. The cellular internalization of nanomedicine is dependent on several factors such as size, stiffness, structure, and surface charge.[65] The cellular uptake study was performed in the H-1975 cell line due to its prominent results in cytotoxicity. The mutant lung cancer

Table 5 IC_{50} and selective index (SI) of DM solution, DM-loaded PEGylated cubosomes, and blank PEGylated cubosomes on RPE1, A549, and H-1975 cell lines

	IC_{50} (μg mL^{-1}, mean ± SD, n = 3)			
	RPE 1	A-549	H-1975	Selective index (SI)
DM	31.30 ± 1.50	20.40 ± 1.10	16.29 ± 0.64	1.92
DM-loaded PEGylated cubosomes	163.30 ± 3.70	10.20 ± 0.15	2.11 ± 0.08	77.39
PEGylated cubosomes	700.00 ± 20	500.00 ± 30.00	694.28 ± 27.40	1.00

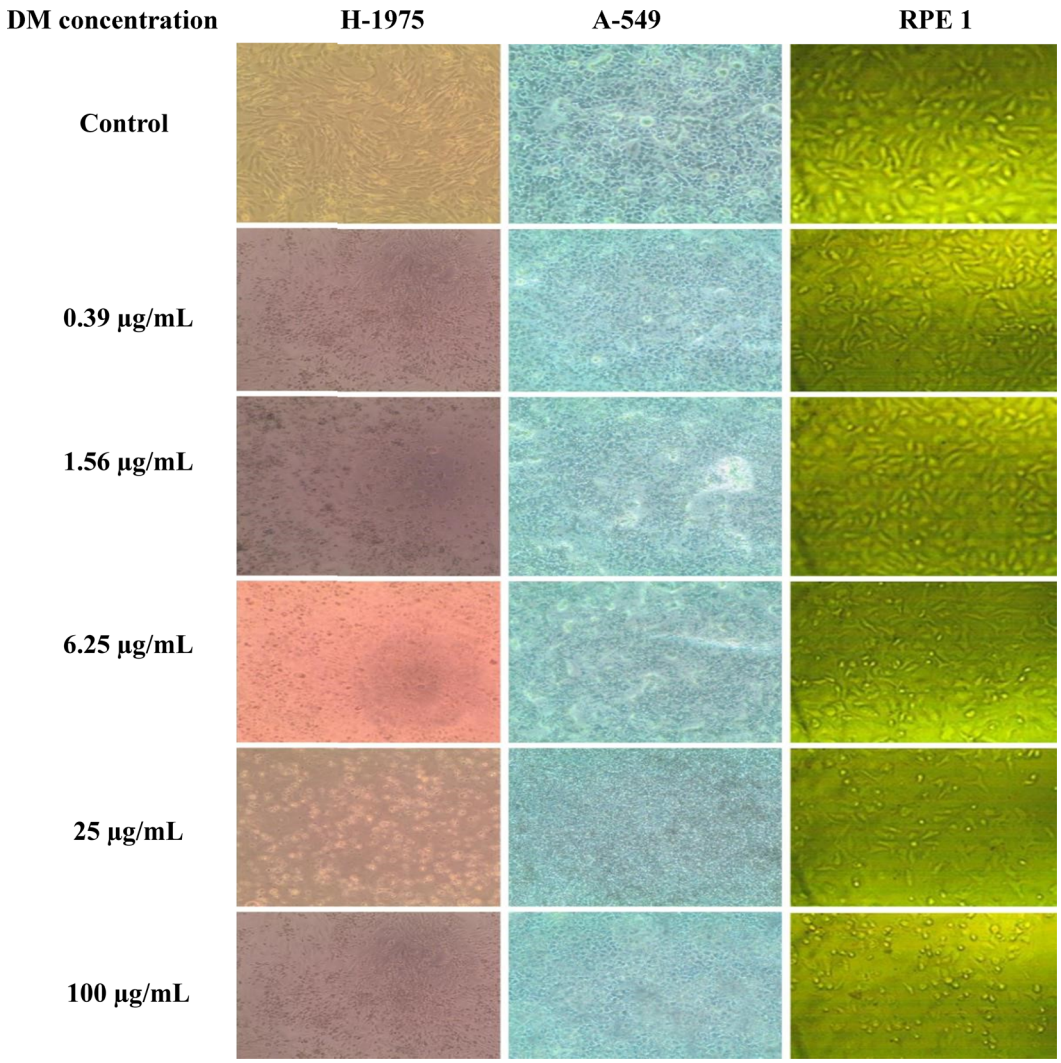

Fig. 8 Morphological changes in RPE1, A-549, and H-1975 cell lines after 48 h incubation with different concentrations of F5 for 48 h.

cell line showed a huge statistically significant difference ($P \leq 0.0001$) between the free DM (less than 1% cellular internalization) and DM-loaded PEGylated cubosomes which achieved a cellular uptake of 83.50%, indicating a highly favorable outcome for the efficient targeting of DM into NSCLC highly resistant cells.

The explanation for the outstanding results is the structure of the formulated PEGylated cubosomes which may enhance cellular uptake by two mechanisms. The first typically involves internalization through rapid non-specific phagocytosis and enhanced dug endocytosis due to the presence of PEG 6000 chains that can facilitate the interaction of cubosomes with the cell membrane, promoting endocytosis. The other mechanism is that GMO may cause membrane fusion between cells and cubosomes owing to known cellular interactions with lipid nanoparticles possessing different internal nanostructures such as liposomes, hexosomes, and cubosomes.[66] Also, oleic acid facilitates the fusion of cubosomes with cancer cell membranes,

particularly in cells with higher fatty acid uptake mechanisms. Cancer cells often have an altered lipid metabolism and are more likely to absorb oleic acid, making cubosomes with OA more likely to be taken up by cancer cells compared with normal cells.[67]

3.9.3. Cell cycle analysis. Flow cytometry analysis was utilized to assess the impact of DM-loaded PEGylated cubosomes on the cell cycle progression of H-1975 mutant lung cancer cells compared with free DM solution. As illustrated in Fig. 9 DM-loaded PEGylated cubosomes significantly inhibited the proliferation of H-1975 cells by inducing G1/S phase arrest.[68] Furthermore, the relative % of cells arrested in the cell cycle was significantly higher compared with control untreated cells. DM-loaded PEGylated cubosomes exhibited a substantial increase in the proportion of cells in the G0/G1 phase, exceeding the effect observed with free DM. This G0/G1 phase cell cycle arrest was accompanied by a simultaneous decrease in the % of cells in the S and G2/M phases following treatment with DM-loaded PEGylated cubosomes (Tables 6 and 7). These findings indicate that cubosomal nanoparticle treatment hindered the cell cycle progression of lung cancer cells, leading to accumulation in the G0/G1 phase. Comparable outcomes were previously reported.[31,69]

Table 6 The effect of free DM and DM PEGylated cubosomes (F5) on the redistribution of growth-arrested H-1975 cells in the different phases of the cell cycle

	DNA content		
	% G1	% G2/M	S
Control cells	46.82	24.05	29.13
Free DM	49.95	16.09	33.16
DM-loaded PEGylated cubosomes (F5)	51.07	14.91	34.02

Table 7 Summary of the percentage of cell apoptosis

	Apoptosis %			
	Total	Early	Late	Necrosis
Control cells	2.61	0.67	0.13	1.81
Free DM	24.96	8.45	13.88	2.63
DM-loaded PEGylated cubosomes	29.77	16.12	9.56	4.09

3.9.4. Cell apoptosis study by flow cytometry. As illustrated in Fig. 10, the top left quadrant (Q1) represents cells undergoing necrosis, the top right quadrant (Q2) depicts cells in late apoptosis and necrosis, the bottom left quadrant (Q3) indicates healthy cells, and the bottom right quadrant (Q4) shows cells in early

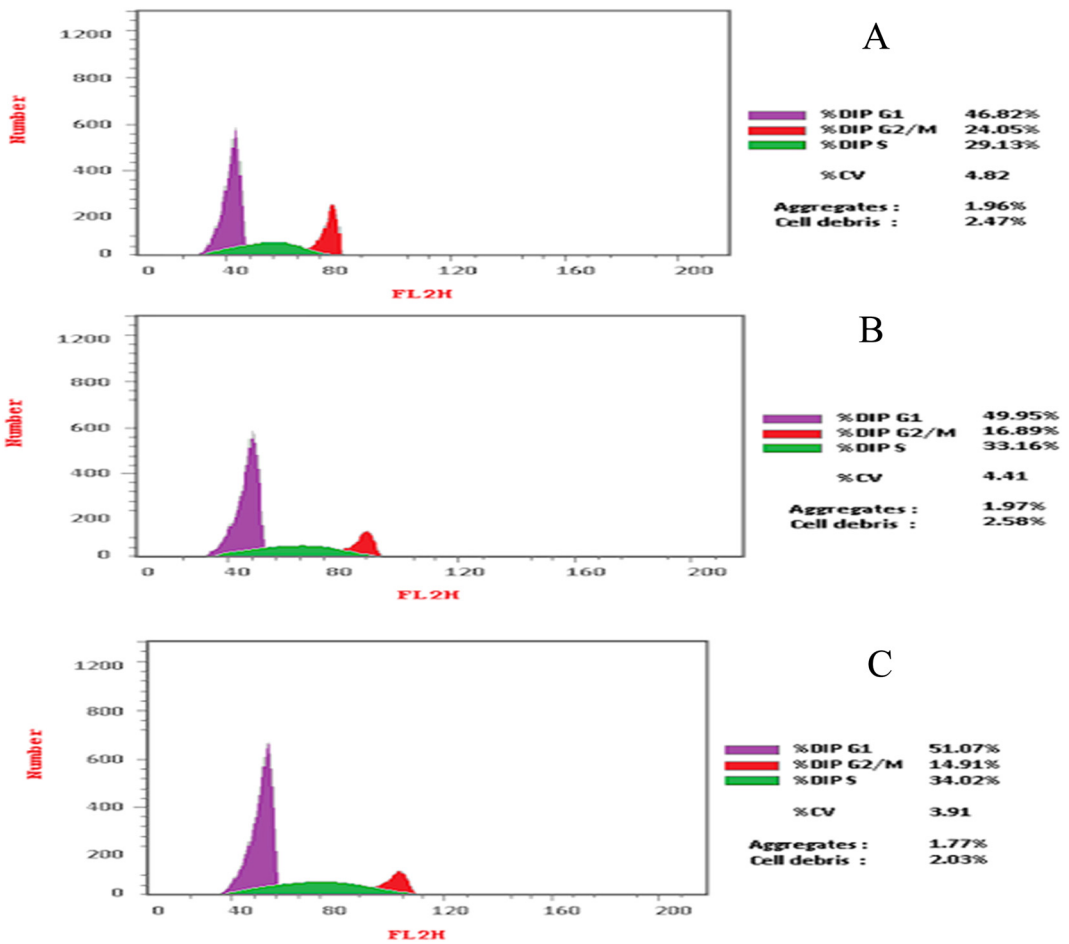

Fig. 9 Flow cytometry cell cycle quantitative analysis of control (A), free DM solution (B), and DM-loaded PEGylated cubosomes (C).

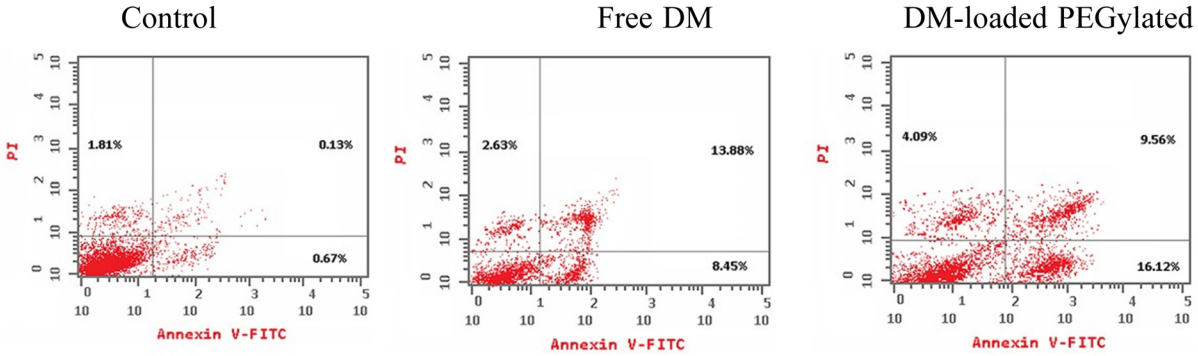

Fig. 10 Cellular apoptosis of H1975 lung cancer cells evaluated *via* flow cytometry using annexin V-FITC staining.

apoptosis. The findings revealed an increase in the total apoptosis rate from 2.61% in the control group to 29.77% in the DM-loaded PEGylated cubosomes group. Importantly, encapsulating DM in cubosomes did not diminish its cytotoxic effect; rather, it enhanced cytotoxicity by a factor of 1.2[31,70] and it could be expected to show greater cytotoxicity than that of the free DM, following prolonged treatments.[62] Flow cytometry analysis results indicated a correlation between apoptosis initiation and changes in cell cycle progression. Increasing evidence suggests that alterations in the cell cycle can either inhibit or promote apoptosis and/or necrosis.[71] This study demonstrated that cell cycle arrest at the G1/S phase led to apoptosis rather than necrosis. Recent reports have highlighted that inhibition of EGFR signaling can induce elevated intracellular ROS levels in cancer cells, thereby triggering apoptosis.[68]

4. Conclusion

pH-sensitive PEGylated cubosomal nanoparticles loaded with DM were successfully formulated utilizing the pH-dependent ionization state of OA. The optimized formulation (F5) demonstrated a small particle size with low polydispersity and high stability. *In vitro* drug release studies revealed a biphasic release profile, with pH-triggered properties as the drug was extensively released in an acidic medium compared with minimal release at normal physiological pH. A prominent cytotoxic efficacy against the H-1975 mutant cell line with a diminished effect on normal epithelial cells proved the high targeting efficiency with minimal hazards. Furthermore, cell cycle analysis confirmed that the antitumor activity primarily involves arresting cells in the G0/G1 phase, followed by the induction of cellular apoptosis.

Overall, the DM-loaded cubosomal dispersion is anticipated to effectively inhibit tumor progression at lower doses than conventional DM, potentially minimizing treatment-related side effects. Nonetheless, further investigations are urgently required to substantiate these findings regarding the antitumor potential of cubosomal nanoparticles *in vivo*.

Future perspectives

Additional preclinical studies, including pharmacokinetic and pharmacodynamic evaluations using appropriate animal models, are planned. These results will guide future efforts to conduct comprehensive clinical investigations for this patient population.

Author contributions

Mohamed Nasr: conceptualization, formal analysis, supervision, and writing – reviewing and editing. Rania Mokhtar: methodology, material preparation, data collection, and writing. Rania S. Abdel-Rashid: conceptualization, supervision, and writing – reviewing and editing.

Data availability

Data will be made available upon request.

Conflicts of interest

The authors declare no competing interests.

Acknowledgements

This research was partially supported by the Scientific Research Funding Authority at Helwan University, whose contribution is gratefully acknowledged. The authors are thankful to Gattefosse (France) for providing the gift sample of glyceryl monooleate.

References

1 A. Pandi, *et al.*, A Brief Review on Lung Cancer, *Int. J. Pharma Res. Health Sci.*, 2016, **4**, 907–914.
2 J. Rivera-Concepcion, D. Uprety and A. A. Adjei, Challenges in the Use of Targeted Therapies in Non-Small Cell Lung Cancer, *Cancer Res. Treat.*, 2022, **54**, 315–329, DOI: **10.4143/crt.2022.078** Preprint at .
3 C. Zappa and S. A. Mousa, Non-small cell lung cancer: Current treatment and future advances, *Transl. Lung Cancer Res.*, 2016, **5**, 288–300.

4 G. Metro and L. Crinò, Advances on EGFR mutation for lung cancer, *Transl. Lung Cancer Res.*, 2012, **1**, 5–13, DOI: **10.3978/j.issn.2218-6751.2011.12.01** Preprint at .
5 V. Smidova, *et al.*, Nanomedicine of tyrosine kinase inhibitors, *Theranostics*, 2021, **11**, 1546–1567, DOI: **10.7150/thno.48662** Preprint at .
6 S. Satapathy and C. S. Patro, Solid Lipid Nanoparticles for Efficient Oral Delivery of Tyrosine Kinase Inhibitors: A Nano Targeted Cancer Drug Delivery, *Adv. Pharm. Bull.*, 2022, **12**, 298–308, DOI: **10.34172/apb.2022.041** Preprint at .
7 Y. T. Lee, Y. J. Tan and C. E. Oon, Molecular targeted therapy: Treating cancer with specificity, *Eur. J. Pharmacol.*, 2018, **834**, 188–196, DOI: **10.1016/j.ejphar.2018.07.034** Preprint at .
8 M. Johnson, M. C. Garassino, T. Mok and T. Mitsudomi, Treatment strategies and outcomes for patients with EGFR-mutant non-small cell lung cancer resistant to EGFR tyrosine kinase inhibitors: Focus on novel therapies, *Lung Cancer*, 2022, **170**, 41–51, DOI: **10.1016/j.lungcan.2022.05.011** Preprint at .
9 C. S. Tan, D. Gilligan and S. Pacey, Treatment approaches for EGFR-inhibitor-resistant patients with non-small-cell lung cancer, *Lancet Oncol.*, 2015, **16**, e447–e459, DOI: **10.1016/S1470-2045(15)00246-6** Preprint at .
10 M. Shirley, Dacomitinib: First Global Approval, *Drugs*, 2018, **78**, 1947–1953.
11 J. E. Shin, *et al.*, Real-world data of dacomitinib as first-line treatment for patients with EGFR-mutant non-small-cell lung cancer, *Sci. Rep.*, 2025, **15**, 4593.
12 CHMP. Committee for Medicinal Products for Human Use (CHMP) Assessment Report., 2019, **https://www.ema.europa.eu/contact**.
13 B. García-Pinel, *et al.*, Lipid-based nanoparticles: Application and recent advances in cancer treatment, *Nanomaterials*, 2019, **9**, 638, DOI: **10.3390/nano9040638**.
14 R. M. Zaki, *et al.*, Formulation of Chitosan-Coated Brigatinib Nanospanlastics: Optimization, Characterization, Stability Assessment and In-Vitro Cytotoxicity Activity against H-1975 Cell Lines, *Pharmaceuticals*, 2022, **15**, 348, DOI: **10.3390/ph15030348**.
15 B. B. Alsulays, M. K. Anwer, G. A. Soliman, S. M. Alshehri and E. S. Khafagy, Impact of penetratin stereochemistry on the oral bioavailability of insulin-loaded solid lipid nanoparticles, *Int. J. Nanomed.*, 2019, **14**, 9127–9138.
16 J. Liu, *et al.*, PH-Sensitive nano-systems for drug delivery in cancer therapy, *Biotechnol. Adv.*, 2014, **32**, 693–710, DOI: **10.1016/j.biotechadv.2013.11.009** Preprint at .
17 L. Shi, *et al.*, Effects of polyethylene glycol on the surface of nanoparticles for targeted drug delivery, *Nanoscale*, 2021, **13**, 10748–10764, DOI: **10.1039/d1nr02065j** Preprint at .
18 A. E. Ashour, *et al.*, Physical pegylation enhances the cytotoxicity of 5-fluorouracil-loaded PLGA and PCL nanoparticles, *Int. J. Nanomed.*, 2019, **14**, 9259–9273.
19 P. Mishra, B. Nayak and R. K. Dey, PEGylation in anti-cancer therapy: An overview, *Asian J. Pharm. Sci.*, 2016, **11**, 337–348, DOI: **10.1016/j.ajps.2015.08.011** Preprint at .
20 R. Varghese, S. Salvi, P. Sood, B. Kulkarni and D. Kumar, Cubosomes in cancer drug delivery: A review, *Colloids Interface Sci. Commun.*, 2022, **46**, 100561, DOI: **10.1016/j.colcom.2021.100561**.
21 M. A. S. Abourehab, *et al.*, Cubosomes as an emerging platform for drug delivery: a review of the state of the art, *J. Mater. Chem. B*, 2022, **10**, 2781–2819, DOI: **10.1039/d2tb00031h**.
22 A. A. El-Shenawy, *et al.*, Anti-Tumor Activity of Orally Administered Gefitinib-Loaded Nanosized Cubosomes against Colon Cancer, *Pharmaceutics*, 2023, **15**, 680.
23 S. W. Jeon, H. S. Jin and Y. J. Park, Formation of Self-Assembled Liquid Crystalline Nanoparticles and Absorption Enhancement of Ω-3s by Phospholipids and Oleic Acids, *Pharmaceutics*, 2022, **14**, 68, DOI: **10.3390/pharmaceutics14010068**.
24 F. Giulitti, *et al.*, Anti-tumor Effect of Oleic Acid in Hepatocellular Carcinoma Cell Lines via Autophagy Reduction, *Front. Cell Dev. Biol.*, 2021, **9**, 629182, DOI: **10.3389/fcell.2021.629182**.
25 M. Nakano, *et al.*, Dispersions of liquid crystalline phases of the monoolein/oleic acid/pluronic F127 system, *Langmuir*, 2002, **18**, 9283–9288.
26 L. Jiang, *et al.*, Oleic acid induces apoptosis and autophagy in the treatment of Tongue Squamous cell carcinomas, *Sci. Rep.*, 2017, **7**, 11277, DOI: **10.1038/s41598-017-11842-5**.
27 C. Carrillo, M. Cavia, M. del and S. R. Alonso-Torre, Efecto antitumoral del ácido oleico; mecanismos de acción; revisión científica, *Nutr. Hosp.*, 2012, **27**, 1860–1865, DOI: **10.3305/nh.2012.27.6.6010** Preprint at .
28 M. Nasr, H. Younes and R. S. Abdel-Rashid, Formulation and evaluation of cubosomes containing colchicine for transdermal delivery, *Drug Delivery Transl. Res.*, 2020, **10**, 1302–1313.
29 M. Nasr, M. K. Ghorab and A. Abdelazem, *In vitro* and *in vivo* evaluation of cubosomes containing 5-fluorouracil for liver targeting, *Acta Pharm. Sin. B*, 2015, **5**, 79–88.
30 K. Kumari, P. Thakur, S. Warde, V. Munipalli and R. M. Singh, HPLC Method Development and Validation for Quantitative Estimation of Dacomitinib in Pharmaceuticals Dosage Form, *Int. J. Pharm. Pharm. Res.*, 2021, **22**, 606–620.
31 Y. S. Loo, T. Madheswaran, R. Rajendran and R. J. Bose, Encapsulation of berberine into liquid crystalline nanoparticles to enhance its solubility and anticancer activity in MCF7 human breast cancer cells, *J. Drug Delivery Sci. Technol.*, 2020, **57**, 101756, DOI: **10.1016/j.jddst.2020.101756**.
32 F. Hashem, M. Nasr and M. Youssif, Formulation and Characterization of Cubosomes Containing REB for Improvement of Oral Absorption of the Drug in Human Volunteers, *J. Adv. Pharm. Res.*, 2018, **2**, 95–103.
33 H. A. El-Enin and A. H. AL-Shanbari, Nanostructured liquid crystalline formulation as a remarkable new drug delivery system of anti-epileptic drugs for treating children patients, *Saudi Pharm. J.*, 2018, **26**, 790–800.
34 S. M. Patil, S. S. Sawant and N. K. Kunda, Inhalable bedaquiline-loaded cubosomes for the treatment of non-small cell lung cancer (NSCLC), *Int. J. Pharm.*, 2021, **607**, 121046, DOI: **10.1016/j.ijpharm.2021.121046**.

35 A. K. Chettupalli, M. Ananthula, P. R. Amarachinta, V. Bakshi and V. K. Yata, Design, formulation, *in vitro* and *ex vivo* evaluation of atazanavir loaded cubosomal gel, *Biointerface Res. Appl. Chem.*, 2021, **11**, 12037–12054.

36 A. E. Eldeeb, S. Salah and M. Ghorab, Formulation and evaluation of cubosomes drug delivery system for treatment of glaucoma: *Ex vivo* permeation and *in vivo* pharmacodynamic study, *J. Drug Delivery Sci. Technol.*, 2019, **52**, 236–247.

37 X. Zeng, *et al.*, Construction of pH-sensitive targeted micelle system co-delivery with curcumin and dasatinib and evaluation of anti-liver cancer, *Drug Delivery*, 2022, **29**, 792–806.

38 X. Zeng, *et al.*, pH-Responsive Hyaluronic Acid Nanoparticles for Enhanced Triple Negative Breast Cancer Therapy, *Int. J. Nanomed.*, 2022, **17**, 1437–1457.

39 J. Xu, *et al.*, HER2 overexpression reverses the relative resistance of EGFR-mutant H1975 cell line to gefitinib, *Oncol. Lett.*, 2016, **12**, 5363–5369.

40 M. Nasr, F. Hashem, M. Teiama, N. Tantawy and R. Abdelmoniem, Folic acid grafted mixed polymeric micelles as a targeted delivery strategy for tamoxifen citrate in treatment of breast cancer, *Drug Delivery Transl. Res.*, 2024, **14**, 945–958.

41 M. Da'i, K. A. Meilinasary, A. Suhendi and S. Haryanti, Selectivity Index of Alpinia galanga Extract and 1′-Acetoxychavicol Acetate on Cancer Cell Lines, *Indones. J. Cancer Chemoprevention*, 2019, **10**, 95–100.

42 N. Sajedi, M. Homayoun, F. Mohammadi and M. Soleimani, Myricetin Exerts its Apoptotic Effects on MCF-7 Breast Cancer Cells through Evoking the BRCA1-GADD45 Pathway, *Asian Pac. J. Cancer Prev.*, 2020, **21**, 3461–3468.

43 M. Chountoulesi, S. Pispas, I. K. Tseti and C. Demetzos, Lyotropic Liquid Crystalline Nanostructures as Drug Delivery Systems and Vaccine Platforms, *Pharmaceuticals*, 2022, **15**, 429, DOI: **10.3390/ph15040429**.

44 T. T. Liu, *et al.*, Preparation, characterization, and evaluation of antitumor effect of Brucea javanica oil cationic nanoemulsions, *Int. J. Nanomed.*, 2016, **11**, 2515–2529.

45 M. Nasr, M. Teiama, A. Ismail, A. Ebada and S. Saber, *In vitro* and *in vivo* evaluation of cubosomal nanoparticles as an ocular delivery system for fluconazole in treatment of keratomycosis, *Drug Delivery Transl. Res.*, 2020, **10**, 1841–1852.

46 S. Kaul, U. Nagaich and N. Verma, Preclinical Assessment of Nanostructured Liquid Crystalline Particles for the Management of Bacterial Keratitis: *in vivo* and Pharmacokinetics Study, *Drug Delivery Transl. Res.*, 2021, **12**, 1719–1737, DOI: **10.1007/s13346-021-01072-8**.

47 M. Zewail, P. M. Passent, M. M. Ali and H. Abbas, Lipidic cubic-phase leflunomide nanoparticles (cubosomes) as a potential tool for breast cancer management, *Drug Delivery*, 2022, **29**, 1663–1674.

48 V. Sethuraman, K. Janakiraman, V. Krishnaswami, S. Natesan and R. Kandasamy, pH responsive delivery of lumefantrine with calcium phosphate nanoparticles loaded lipidic cubosomes for the site specific treatment of lung cancer, *Chem. Phys. Lipids*, 2019, **224**, 104763, DOI: **10.1016/j.chemphyslip.2019.03.016**.

49 E. Nazaruk, A. Majkowska-Pilip and R. Bilewicz, Lipidic Cubic-Phase Nanoparticles—Cubosomes for Efficient Drug Delivery to Cancer Cells, *ChemPlusChem*, 2017, **82**, 570–575.

50 O. Mertins, P. D. Mathews and A. Angelova, Advances in the design of ph-sensitive cubosome liquid crystalline nanocarriers for drug delivery applications, *Nanomaterials*, 2020, **10**, 963, DOI: **10.3390/nano10050963**.

51 S. Rajesh, J. Zhai, C. J. Drummond and N. Tran, Novel pH-Responsive Cubosome and Hexosome Lipid Nanocarriers of SN-38 Are Prospective for Cancer Therapy, *Pharmaceutics*, 2022, **14**, 2175, DOI: **10.3390/pharmaceutics14102175**.

52 S. Phan, W. K. Fong, N. Kirby, T. Hanley and B. J. Boyd, Evaluating the link between self-assembled mesophase structure and drug release, *Int. J. Pharm.*, 2011, **421**, 176–182.

53 A. Angelova, *et al.*, Advances in structural design of lipid-based nanoparticle carriers for delivery of macromolecular drugs, phytochemicals and anti-tumor agents, *Adv. Colloid Interface Sci.*, 2017, **249**, 331–345, DOI: **10.1016/j.cis.2017.04.006** Preprint at .

54 Y. Li, *et al.*, PH Responsiveness of Hexosomes and Cubosomes for Combined Delivery of Brucea javanica Oil and Doxorubicin, *Langmuir*, 2019, **35**, 14532–14542.

55 L. M. Ahmed, K. M. A. Hassanein, F. A. Mohamed and T. H. Elfaham, Formulation and evaluation of simvastatin cubosomal nanoparticles for assessing its wound healing effect, *Sci. Rep.*, 2023, **13**, 17941, DOI: **10.1038/s41598-023-44304-2**.

56 D. Barji, S. M. Patil and N. K. Kunda, Formulation Development of Inhalable Dacomitinib Polymeric Nanoparticles for Non-Small Cell Lung Cancer Treatment, *J. Aerosol Med. Pulm. Drug Delivery*, 2022, **35**, A18–A19.

57 M. N. Musa, *et al.*, Development and evaluation of exemestane-loaded lyotropic liquid crystalline gel formulations, *BioImpacts*, 2017, **7**, 227–239.

58 M. Kazi and M. H. Dehghan, Development of inhalable cubosome nanoparticles of Nystatin for effective management of Invasive Pulmonary Aspergillosis, *Istanbul J. Pharm.*, 2020, **50**, 224–237.

59 M. A. Shetab Boushehri, D. Dietrich and A. Lamprecht, Nanotechnology as a platform for the development of injectable parenteral formulations: A comprehensive review of the know-hows and state of the art, *Pharmaceutics*, 2020, **12**, 1–53, DOI: **10.3390/pharmaceutics12060510**Preprint at .

60 N. Attri, *et al.*, Liposomes to Cubosomes: The Evolution of Lipidic Nanocarriers and Their Cutting-Edge Biomedical Applications, *ACS Appl. Bio Mater.*, 2024, **7**, 2677–2694, DOI: **10.1021/acsabm.4c00153**, Preprint at .

61 T. Reungwetwattana, N. Rohatgi, T. S. Mok and K. Prabhash, Dacomitinib as first-line treatment for EGFR mutation-positive non-small cell lung cancer, *Expert Rev. Precis. Med. Drug Dev.*, 2021, **6**, 161–171.

62 R. K. Thapa, *et al.*, Multilayer-coated liquid crystalline nanoparticles for effective sorafenib delivery to hepatocellular carcinoma, *ACS Appl. Mater. Interfaces*, 2015, **7**, 20360–20368.

63 T. M. Hinton, *et al.*, Bicontinuous cubic phase nanoparticle lipid chemistry affects toxicity in cultured cells, *Toxicol. Res.*, 2014, **3**, 11–22.
64 J. A. Engelman, *et al.*, PF00299804, an irreversible pan-ERBB inhibitor, is effective in lung cancer models with EGFR and ERBB2 mutations that are resistant to gefitinib, *Cancer Res.*, 2007, **67**, 11924–11932.
65 J. B. Strachan, B. P. Dyett, Z. Nasa, C. Valery and C. E. Conn, Toxicity and cellular uptake of lipid nanoparticles of different structure and composition, *J. Colloid Interface Sci.*, 2020, **576**, 241–251.
66 S. L. Yap, *et al.*, Cell interactions with lipid nanoparticles possessing different internal nanostructures: Liposomes, bicontinuous cubosomes, hexosomes, and discontinuous micellar cubosomes, *J. Colloid Interface Sci.*, 2024, **656**, 409–423.
67 S. H. Hwang, Y. Yang, J. H. Jung and Y. Kim, Oleic acid from cancer-associated fibroblast promotes cancer cell stemness by stearoyl-CoA desaturase under glucose-deficient condition, *Cancer Cell Int.*, 2022, **22**, 404, DOI: 10.1186/s12935-022-02824-3.
68 X. Yu, *et al.*, Dacomitinib, a new pan-EGFR inhibitor, is effective in attenuating pulmonary vascular remodeling and pulmonary hypertension, *Eur. J. Pharmacol.*, 2019, **850**, 97–108.
69 A. Cytryniak, *et al.*, Cubosomal Lipid Formulation for Combination Cancer Treatment: Delivery of a Chemotherapeutic Agent and Complexed α-Particle Emitter 213Bi, *Mol. Pharmacol.*, 2022, **19**, 2818–2831.
70 S. Pushpa Ragini, *et al.*, Novel bioactive cationic cubosomes enhance the cytotoxic effect of paclitaxel against a paclitaxel resistant prostate cancer cell-line, *J. Colloid Interface Sci.*, 2023, **649**, 966–976.
71 A. Moin, *et al.*, Formulation, characterization, and cellular toxicity assessment of tamoxifen-loaded silk fibroin nanoparticles in breast cancer, *Drug Delivery*, 2021, **28**, 1626–1636.